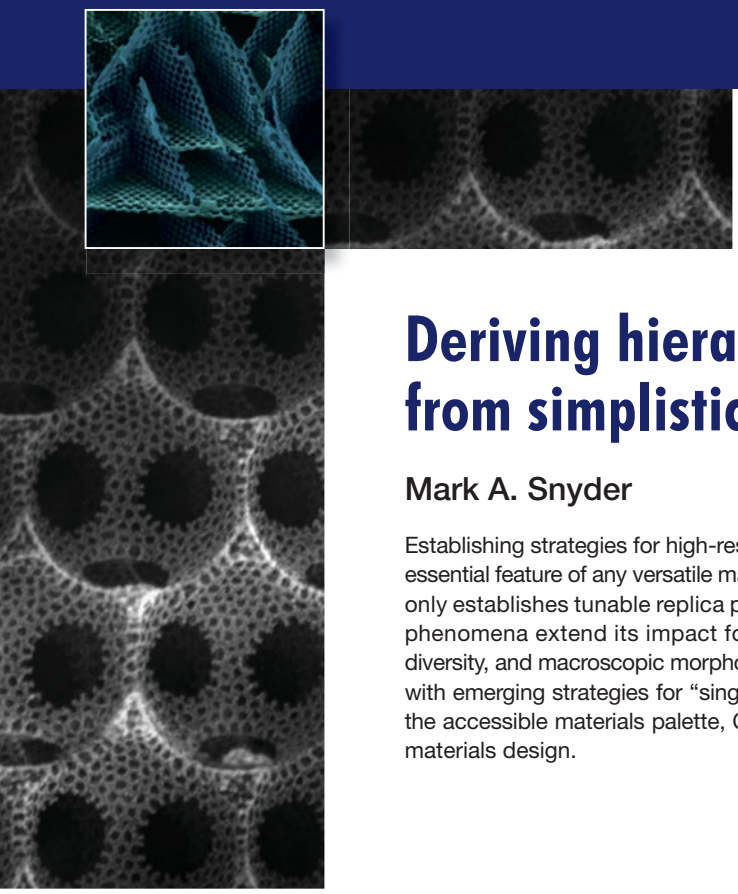


Deriving hierarchical complexity from simplistic colloidal templates

Mark A. Snyder

Establishing strategies for high-resolution micrometer to subnanometer structural control is an essential feature of any versatile materials design paradigm. Colloidal crystal (CC) templating not only establishes tunable replica pore topologies, but interfacial- and confinement-mediated phenomena extend its impact for tailoring properties such as pore hierarchy, topological diversity, and macroscopic morphology, as well as nucleation, growth, and crystallinity. Coupled with emerging strategies for "single-pot" template-replica co-assembly and efforts to expand the accessible materials palette, CC-templating offers promise for application-driven, rational materials design.

Introduction

Multiscale templating strategies capable of directing assembly of molecules, macromolecules, nanoparticles, or microparticles have promise for realizing hierarchical structuring in amorphous to crystalline materials and across a continuum of scales.[1,2] While no single templating strategy enables comprehensive control among all scales or material classes, **Figure 1**a highlights the range of scales that can be accessed by structural "soft" and "hard" templating, spanning molecular to macroscopic dimensions. Soft molecular porogens can template micropores (e.g., in zeolites), or they can be assembled into macromolecular structures such as micelles and ordered lyotropic liquid-crystal phases (e.g., cubic, hexagonal, lamellar) that can be exploited as sacrificial templates of replica mesopores. As such, soft templating offers pore-size control spanning <1 nm–15 nm and topological diversity, illustrated by 200+ microporous zeolite frameworks and various mesopore symmetries.[3–6] Hard templating,[7,8] the process whereby a preformed structured solid serves as a mold for casting the synthetic replication of a distinct secondary phase (replica) prior to template removal, decouples the template formation and replication processes. This circumvents the uncertain synthesis–structure relations often plaguing soft strategies, caused by the common unpredictability of complex template–precursor interactions and sensitivity to process and solution conditions. This decoupling also helps expand the replica compositions accessible by the hard-templating approach.

Ordered mesoporous materials (OMMs [e.g., mesoporous silicas]) have been commonly exploited as sacrificial hard templates for casting other porous phases (e.g., mesoporous carbon).[7,8] In these cases, filling of the OMM pores with a distinct secondary phase prior to the template sacrifice yields replicas, the walls and pores of which are templated, respectively, by the pores and walls of the OMM template. Yet, pore formation in OMMs themselves occurs via soft templating, which provides limited control over OMM pore wall thickness, and thus replica pore size.

Colloidal crystals (CCs), structures comprised of three-dimensionally ordered assemblies of colloidal particles, offer an alternative versatile platform for hard templating. Specifically, preformed CCs, comprised of polymeric (e.g., polystyrene [PS], poly(methyl methacrylate) [PMMA]) or inorganic (e.g., SiO_2) micro- to nanoparticles (1) offer three-dimensional (3D)-interconnected interstices and continuous particle surfaces for hosting, respectively, volumetric infiltration or conformal, interfacial coating by molecular replica precursors; (2) confine the reaction and solidification of infiltrated molecular precursors within the interstitial volume (i.e., volumetric replicas) or on the surfaces of the template (i.e., interfacial replicas) during synthesis of a distinct replica phase; (3) stabilize replica pores against collapse during composite processing; and (4) leave behind spherical replica pore bodies upon removal of the template of a size commensurate with the

Mark A. Snyder, Department of Chemical and Biomolecular Engineering, Lehigh University, USA; snyder@lehigh.edu
doi:10.1557/mrs.2016.187

© 2016 Materials Research Society

https://doi.org/10.1557/mrs.2016.187 Published online by Cambridge University Press

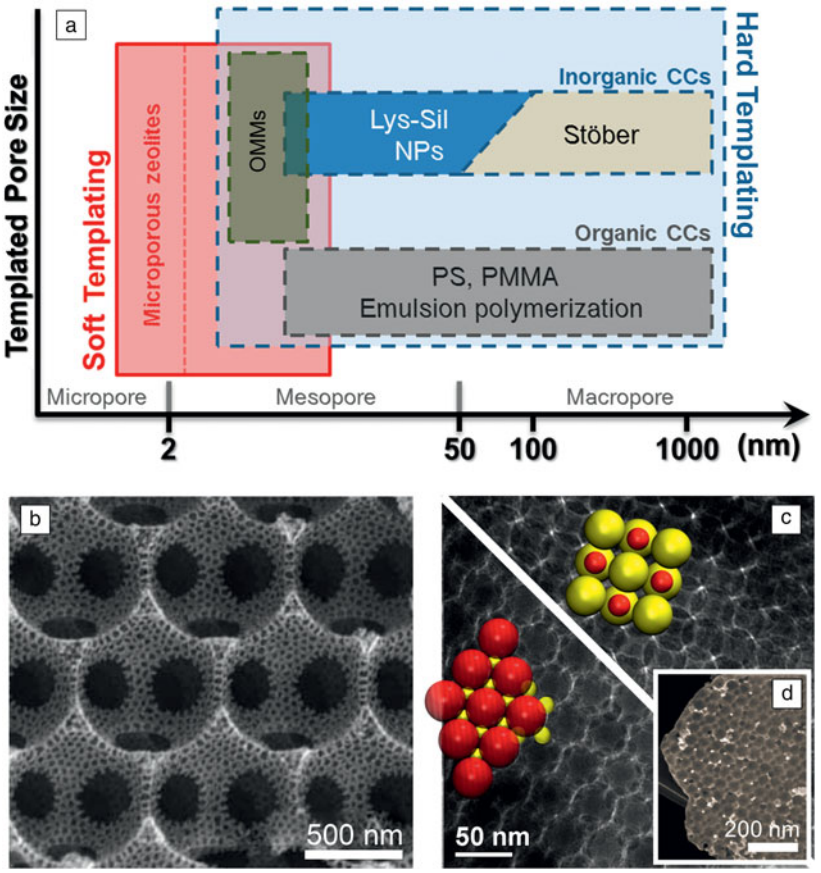


Figure 1. (a) Schematic comparing characteristic soft and hard templating scales, with "hard" templating achieved by sacrificial ordered mesoporous materials (OMMs) or colloidal crystals (CCs) comprised of either organic constituent particles (e.g., polystyrene [PS], poly(methyl methacrylate) [PMMA]), derived commonly through emulsion polymerization, or inorganic constituent nanoparticles (NPs) or microparticles synthesized, respectively, by amino acid (e.g., lysine)-mediated methods ("Lys-Sil" silica NPs) or conventional Stöber methods. (a) The access to hierarchical pores permitted by multimodal CCs comprised of (b) largely or (c) subtly disparate constituent particles, with the co-assembly of the latter yielding packing stoichiometries: AB (top) and AB_2 (bottom), dictated by particle size ratio. Both (b) volumetric replication (carbon) and (d) templating of anisotropic crystal growth along CC symmetry planes (CC-dimpled gold sheets) is possible. (b) Adapted with permission from Reference 22. © 2010 Royal Society of Chemistry. (c) Adapted with permission from Reference 26. © 2014 American Chemical Society. (d) Adapted with permission from Reference 27. © 2012 American Chemical Society.

constituent CC particles. These templated pore bodies are three-dimensionally interconnected by smaller "pore windows" formed by exclusion of the molecular replica precursor from points of interparticle contact.[9] Numerous comprehensive reviews have been published over the past decade spanning CC assembly[10] to sacrificial CC-based templating.[11–16]

In this article, the juxtaposition of the geometric simplicity of CCs with the surprising hierarchical complexity they may cast within replicas is highlighted. Closure of the gap in accessible pore sizes posed by conventional hard templating, emergence of CC-imposed confinement and interfacial phenomena for tuning morphologic to crystallographic replica properties, and progress toward bottom-up CC-templating of compositionally diverse hierarchical materials are reviewed.

Closing the gap in CC templating

CCs comprised of micron- or submicron-size particles have been routinely exploited as sacrificial templates of three-dimensionally ordered macroporous (3DOM) replicas characterized by 3D-interconnected micron- to submicron spherical pore bodies,[11] with the stability of inorganic CCs bolstering pore topology under high-temperature processing. Conventional Stöber[17] synthesis yields monodisperse micron and submicron silica particles through controlled hydrolysis of silicon alkoxides under basic conditions. Only within the last decade has a synthesis strategy been identified wherein highly monodisperse silica nanoparticles as small as ~5 nm are realized through a facile amino acid-mediated approach. The resulting "Lys-Sil" nanoparticles, named for their derivation from lysine-mediated aqueous-phase hydrolysis of a silicon alkoxide precursor,[18–20] can be tuned in size within a once elusive range (ca. 5–100 nm). This facile accessibility of smaller particle scales and, ultimately, the further ability to convectively assemble these particles into siliceous nanoparticle crystalline superlattices with face-centered-cubic (fcc) symmetry,[20,21] has helped close the size gap in CC-based templating from macroporous (3DOM) toward three-dimensionally ordered mesoporous (3DOm) replicas with sub-10 nm to ~50 nm spherical pore bodies, and pore windows approaching near-micropore dimensions.[9]

Topological hierarchy and diversity through modular CC templating

Strategies for expanding the topological diversity and hierarchy in size of replica pores, beyond the fcc arrangement and monodisperse sizes templated by unimodal CCs, are important for meeting application needs. Tuning the specific hierarchy of pore sizes can be accomplished by assembling template building blocks that match sought-after scales. However, the practical arrangement of these disparate-sized particles into multimodal structures suitable for templating specific dimensionality, interconnectivity, and spatial arrangement of replica pores, requires their engineered assembly. Specifically, sequential assembly is possible when significantly disparate pore scales, and thus particle scales are sought (Figure 1b) with assemblies of the largest particles serving as 3D hosts for subsequent assembly of smaller particles.[13,22]

Sequential assembly methods begin to fail, however, as the distinction between pore scales, and thus that of the disparate template particles, narrows. Simultaneous co-assembly of constituent particles is then required to realize multimodal CC templates characterized by varied solid stoichiometries, as has

https://doi.org/10.1557/mrs.2016.187 Published online by Cambridge University Press

been demonstrated with stabilized microparticles or submicrometer particles of various compositions[23–25] and, most recently, native Lys-Sil nanoparticles[26,27] (Figure 1c). The latter assemblies hold promise for enhancing mesoscale pore hierarchy during volumetric replication, and have been exploited for the templating of hierarchically dimpled gold flakes along CC symmetry planes[27] (Figure 1d).

Growing complexity from simplicity: CC-mediated multiscale engineering

The large, tailorable-chemistry surface areas and tunable interstitial pore size of CCs have emerged, respectively, as interfacial- and confinement-based tools for multiscale tailoring of replica complexity.

Macroscale: Morphology control by CC-mediated mass transport

CC-imposed volumetric confinement can impact the interstitial transport of reacting (i.e., polymerizing, crystallizing) molecular precursors during replication as a result of concomitant reductions in the interstitial free volume of the template. In addition, electrostatic and hydrogen bonding interactions between the CC surface and replica species can limit their interstitial mobility.[15] This can lead to localized species gradients,[28] modulation of phase transformations,[29,30] and selection between volumetric (i.e., space-filling) and interfacial (i.e., conformal) CC replication.[30] These effects are commonly manifested as macroscopic morphological differences in the synthesized materials that distinguish templated from untemplated materials.

Specifically, Stein and co-workers[29,30] demonstrated this for CeO_2, Fe_2O_3, and Mn_3O_4 ceramics undergoing step-growth polymerization and spinodal decomposition within negatively charged PMMA CCs. A continuum of distinct and diverse macroscopic morphologies was observed and concluded to be based upon the interplay of varying degrees of polymerization, degree of reactant imbalance, and interactions with the CC template. With increasing extent of reaction and decreasing reactant imbalance, the macroscopic morphology was found to change continuously among a diverse set of 3DOM structures, including continuous 3DOM monoliths, open bicontinuous networks, interconnected microspheres, dense bicontinuous structures, and cracked monoliths, several of which are shown in **Figure 2**a–c. This diversity of structures was not observed in the absence of the template.

At smaller scales, CC surface-mediation of ion transport can also modulate morphology, as demonstrated for electrodeposition of 3DOM Cu_2O crystallites[28] within a PS CC. H^+ and Cu^{2+}/Cu^+ ion transport limits lead, respectively, to localized pH reduction and ion concentration gradients within the template that enhance Cu_2O branching and cause distinct apex formation (Figure 2d); phenomena and features that are

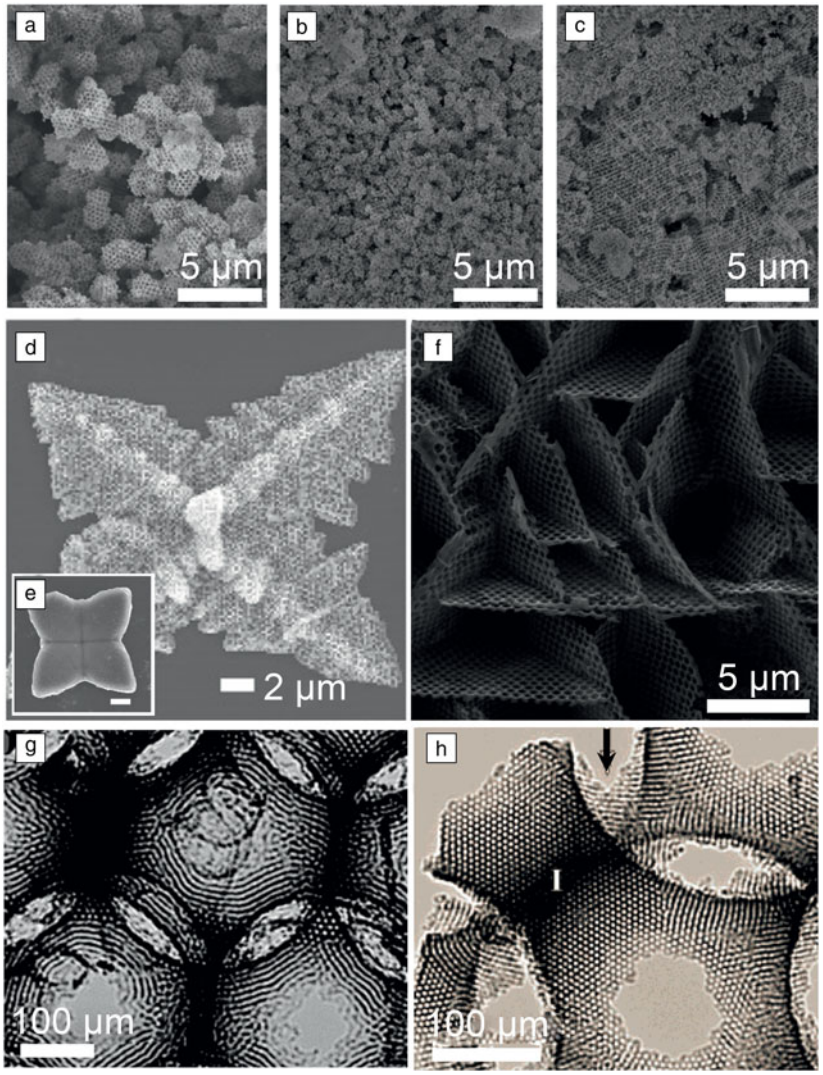


Figure 2. Colloidal crystal (CC)-templated control over (a–c) macroscopic morphology in three-dimensionally ordered macroporous (3DOM) CeO_2, with a decreasing degree of polymerization induced by decreasing the gelation temperature and time: (a) 90°C (16 h), (b) 80°C (16 h), and (c) 40°C (24 h). (d) Branching/apex formation in 3DOM Cu_2O in cupric acetate buffer relative to (e) the untemplated structure, and (f) anisotropic growth of 3DOM ZnO "house of cards" along CC symmetry planes. Panels (g–h) depict mesoscale pore topology of 3DOM SiO_2 derived from soft templating by (g) polymeric surfactant Pluronic P123 and (h) nonionic surfactant Brij 56, showing respective mesopore orientation parallel or perpendicular (hexagonal array) to the macropore (sacrificed template) surface, and mesostructure modulation at constraints (arrow) relative to less-confined octahedral interstices of the template (Region I). (a–c) Adapted with permission from Reference 30. © 2014 American Chemical Society. (d–e) Adapted with permission from Reference 28. © 2014 American Chemical Society. (f) Adapted with permission from Reference 31. © 2008 Royal Society of Chemistry. (g–h) Adapted with permission from Reference 34. © 2007 American Chemical Society.

https://doi.org/10.1557/mrs.2016.187 Published online by Cambridge University Press

either absent or suppressed in their untemplated counterparts (Figure 2e). Finally, in the presence of low-energy CC symmetry planes, such transport effects combine with interfacial phenomena to template growth of low-dimensional, hierarchically intersecting "house of cards" architectures, an example of which is shown in Figure 2f for ZnO.[31,32]

Mesoscale: CC-mediated hierarchical mesostructuring

Motivated by the continuum of scales accessible by hard and soft templating (Figure 1a), their modular combination is commonly employed to dual-template hierarchical structures.[33] Figure 2g–h shows representative soft-templated mesopore topologies within siliceous 3DOM replicas of PMMA CCs.[34] The variation in pore orientation parallel or perpendicular to the 3DOM pore surface, a general soft-templating phenomenon observed with other precursors (e.g., metal alkoxides, carbons)[12] and within two-dimensional films,[35,36] results from the segregation of mesoscale porogens (i.e., micelles) toward the CC template surfaces, a phenomenon driven by interfacial forces. These interfacial effects translate to complex pore orientation under confinement within the 3D-interconnected octahedral and tetrahedral pore topology of CCs. The 3D-interconnected pore topology of CCs thus enables control over mesophase order through volumetric confinement and even surface curvature, the latter of which modulates lattice spacing.

Microscale: Interface and confinement-mediated crystallization

Interstitial confinement and CC interfaces also play a key role in templated nucleation and crystallization. 3DOM/3DOm replica metal oxides (e.g., TiO_2, ZrO_2, SnO_2, CeO_2) derived from CC-confined solvothermal synthesis reveal that interfacial forces may promote heterogeneous nucleation and anchoring of nanoparticle nuclei,[37] and thereby minimize crystal mobility/coarsening while bolstering metastable polymorphism.[38] The ensuing classical (molecular addition) or nonclassical (oriented attachment) crystal growth results, respectively, in 3DOM/3DOm single crystals or mesocrystals upon template sacrifice, the latter comprised of similarly oriented nanocrystallites rather than a continuous single crystal domain.[37,39,40]

This raises the question of whether crystallization of carbons is equally favored given their promise for novel electrochemical devices. Early reports of siliceous CC replication with mesophase pitch yielded turbostratic carbon (disordered carbon characterized by intertwined graphitic ribbons) under lower-temperature (1000°C) processing, and required high temperatures (2500°C) to stimulate graphene growth without a specific graphitizing catalyst.[41] Recently, Dong and co-workers[42] expanded the CC templating palette to include Fe_3O_4 CC with graphitizing catalytic functionality and a covalently tethered oxalic acid (OA) replica precursor. Lower-temperature (500°C) synthesis of partially graphitic 3DOm structures enables moderate inert heating (1000°C) to achieve robust 3DOm carbon with ultrathin (ca. 2 nm thick) graphene walls, attractive Brunauer-Emmett-Teller surface areas (ca. 1000 $m^2\ g^{-1}$), large pore volumes (ca. 1.8 $cm^3\ g^{-1}$), and CC-tunable mesopores (ca. 8–20 nm) (**Figure 3**a). The strong electrochemical performance of these materials when applied as anodes in Li-ion batteries derives from the hierarchical structure, namely from their unique 3D-interconnected architecture, low resistance to Li ion transport, and reduced barriers for Li intercalation and extraction, owing to the thin walls of the structure.[42]

Toward single-pot CC-replica co-assembly

The holy grail for complex materials synthesis is co-assembly of molecular and particulate building blocks with structure-directing moieties to rationally and simultaneously engineer composition, structure, and function. The work of Dong and co-workers,[42] wherein covalent attachment of precursors to the assembling particles circumvents template preformation, highlights a viable single-pot CC-templating strategy. Earlier reports[43,44] demonstrated how convective assembly of micrometer and nanometer particles from solutions containing solvated molecular replica precursors (e.g., carbon, metal [Si, Ti, Ge] alkoxides),[45–48] offers a single-step approach to volume- or interfacially infiltrated, ordered CCs and, following processing and template removal, to crack-free 3DOM architectures as well as hierarchical 3DOm structures.

In one study, adsorption of carbon molecular precursors to the surface of dispersed template nanoparticles during their convective assembly into CCs was found to modulate the assembly and templating.[44] Upon polymerization and carbonization of the carbon molecular replica precursors followed by template removal, replica structures were realized that bear two independent and uniquely interdigitated pore topologies: conventional 3DOm pores templated by the constituent CC particles and a second set of pores associated with the CC interstices (Figure 3b). Extension of these strategies to include the co-assembly of colloidal template particles with nanoparticulate precursors (e.g., TiO_2,[49] yttrium-stabilized zirconia[50]), rather than molecular precursors, have even begun establishing a single-pot route to 3DOM nanocrystalline mesocrystals, thus underscoring the versatility of this approach.

Expanding the compositional palette of direct and indirect CC-templating

CC replicas themselves[19,51] have also been successfully employed as sacrificial scaffolding for the growth of structured 3D particle superlattices comprised of materials that may otherwise elude synthesis as monodisperse particles, and preclude direct assembly (e.g., carbon, SnO_2, TiO_2, mixed oxides [Figure 3c];[51] crystalline microporous zeolites [Figure 3e[19,52]]). Scaffolding their growth yields single- or near-single-crystalline interconnectivity between constituent particles. In the case of electrochemically relevant materials, excellent battery performance (Figure 3d) has been reported for SnO_2 nanoparticle

https://doi.org/10.1557/mrs.2016.187 Published online by Cambridge University Press

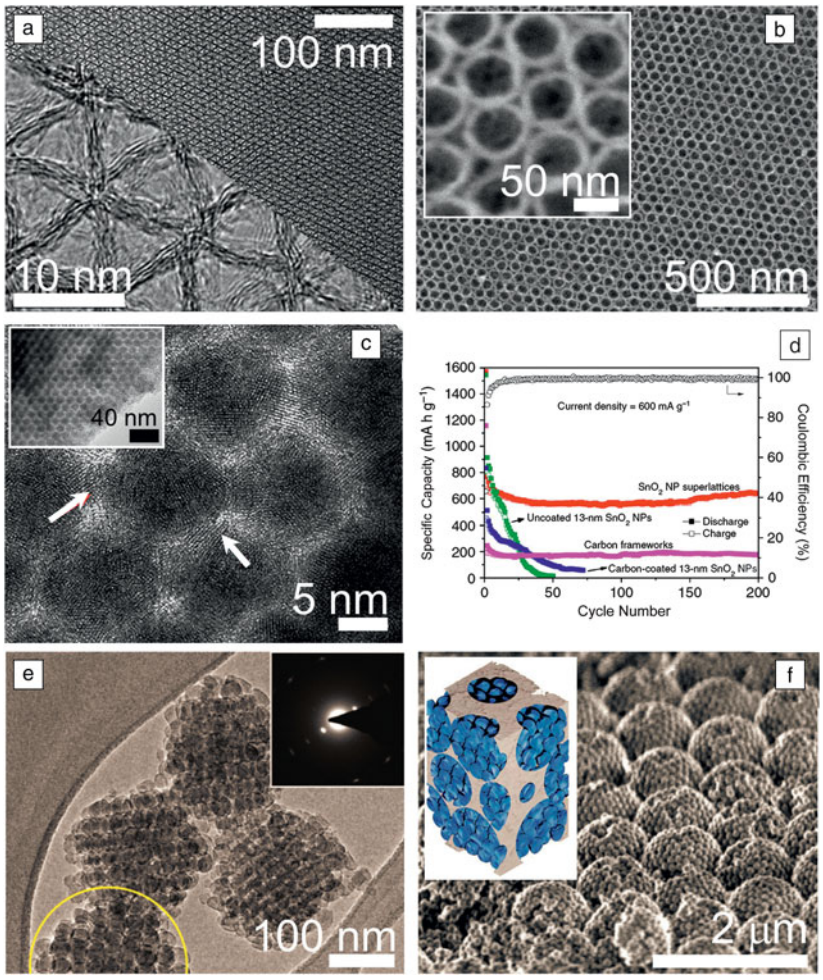


Figure 3. Extending the colloidal crystal templating strategy to new materials and structures, including (a) three-dimensionally ordered mesoporous (3DOm) graphene replication of Fe_3O_4 nanoparticle (NP) superlattices and (b) interdigitated bimodal 3DOm carbon from co-assembly and processing of Lys-Sil template (removed) and glucose precursor. (c) Transmission electron microscope images of a SnO_2 nanoparticle superlattice templated on the 3DOm graphene replica shown in (a), with evidence of crystalline nanoparticulate interconnectivity (arrows) and (d) superior electrochemical cycling performance (measured at a current density of 600 mA g^{-1}) underscored by the high cycling stability and coulombic efficiency relative to the more than 70% lower specific capacity of the native 3DOm graphene template (carbon frameworks) and poor cycling stability of 13-nm SnO_2 nanoparticles synthesized and assembled outside a template when tested in their native (uncoated) and carbon-coated forms. (e) Near-single-crystalline (inset) 3DOm-imprinted (3DOm-i) LTA-type zeolite scaffolded in sacrificed 3DOm carbon, and (f) a double-periodic inverse opal structure (inset, templating schematic). (a) Adapted with permission from Reference 42. © 2015 Wiley. (b) Adapted with permission from Reference 44. © 2014 American Chemical Society. (c–d) Adapted with permission from Reference 51. © 2015 Nature Publishing Group. (e) Adapted with permission from Reference 52. © 2011 American Chemical Society. (f) Adapted with permission from Reference 56. © 2013 Wiley.

superlattices (Figure 3c) grown within the aforementioned CC-templated graphene,[51] owing to enhanced electron transport through crystalline interparticle connections, close proximity to the retained graphene scaffold, and scaffold mediation of SnO_2 volume expansions.

In the case of hierarchically porous structures (e.g., 3DOm-imprinted [3DOm-i] zeolites[19,52,53] [Figure 3e] or mesostructured metal–organic frameworks[54]), scaffolded mesoporosity offers unfettered access to large interfacial areas and tailored diffusion length scales that balance transport and function, and can lead, for example, to activity enhancements as reported for xylose isomerization in 3DOm-i zeolites with a Sn-MFI framework.[55] In addition, complex double-periodic opal or inverse opal SiO_2, TiO_2, Al_2O_3, and carbon structures[56] (Figure 3f) have been realized with analogously hierarchical porosity, but at optically relevant scales, via indirect CC templating of secondary colloidal assemblies. As such, the versatility of direct or indirect CC-templating helps expand the compositional and topological palette for this approach.

Summary

Colloidal crystals offer a versatile framework for tailoring complexity within hierarchical materials spanning replica pore templating to control macroscopic morphology, mesoscopic pore topology and orientation, and nucleation and crystallinity. At the heart of recent advances in CC-templating is the establishment of strategies to complete the continuum of synthetic inorganic nano- to microparticles, enabling modular templating of pore hierarchy and expansion of replica topological diversity. Progress toward CC template-replica co-assembly of hierarchically structured materials underscores the role that CC templating should play in the paradigm shift toward bottom-up rational design and engineering of structurally, functionally, and compositionally complex materials to meet demands of current and emerging needs.

Acknowledgments

M.A.S. gratefully acknowledges support from the US National Science Foundation CAREER Award (Grant CBET-1351613) and Grant DMR-1429359.

References

1. B.-L. Su, C. Sanchez, X.-Y. Yang, in *Hierarchically Structured Porous Materials: From Nanoscience to Catalysis, Separation, Optics, Energy, and Life Science*, B.-L. Su, C. Sanchez, X.-Y. Yang, Eds. (Wiley-VCH, Weinheim, Germany, 2012), pp. 3–27.
2. P. Trogadas, V. Ramani, P. Strasser, T.F. Fuller, M.-O. Coppens, *Angew. Chem. Int. Ed.* **55**, 122 (2016).
3. A. Corma, *Chem. Rev.* **97**, 2373 (1997).
4. M.E. Davis, *Nature* **417**, 813 (2002).
5. A.G. Slater, A.I. Cooper, *Science* **348**, 988 (2015).
6. Y. Wan, D.Y. Zhao, *Chem. Rev.* **107**, 2821 (2007).
7. A.H. Lu, F. Schuth, *Adv. Mater.* **18**, 1793 (2006).
8. R. Ryoo, S.H. Joo, S. Jun, *J. Phys. Chem. B* **103**, 7743 (1999).
9. K.A. Cychosz, X. Guo, W. Fan, R. Cimino, G.Y. Gor, M. Tsapatsis, A.V. Neimark, M. Thommes, *Langmuir* **28**, 12647 (2012).

https://doi.org/10.1557/mrs.2016.187 Published online by Cambridge University Press

10. N. Vogel, M. Retsch, C.-A. Fustin, A. del Campo, U. Jonas, *Chem. Rev.* **115**, 6265 (2015).
11. N.D. Petkovich, A. Stein, in *Hierarchically Structured Porous Materials: From Nanoscience to Catalysis, Separation, Optics, Energy and Life Science*, B.-L. Su, C. Sanchez, X.-Y. Yang, Eds. (Wiley-VCH, Weinheim, Germany, 2012), pp. 55–129.
12. N.D. Petkovich, A. Stein, *Chem. Soc. Rev.* **42**, 3721 (2013).
13. K.R. Phillips, G.T. England, S. Sunny, E. Shirman, T. Shirman, N. Vogel, J. Aizenberg, *Chem. Soc. Rev.* **45**, 281 (2016).
14. A. Stein, F. Li, N.R. Denny, *Chem. Mater.* **20**, 649 (2008).
15. A. Stein, S.G. Rudisill, N.D. Petkovich, *Chem. Mater.* **26**, 259 (2014).
16. B. Fang, J.H. Kim, M.S. Kim, J.S. Yu, *Acc. Chem. Res.* **46**, 1397 (2013).
17. W. Stöber, A. Fink, E. Bohn, *J. Colloid Interface Sci.* **26**, 62 (1968).
18. T.M. Davis, M.A. Snyder, J.E. Krohn, M. Tsapatsis, *Chem. Mater.* **18**, 5814 (2006).
19. W. Fan, M.A. Snyder, S. Kumar, P.S. Lee, W.C. Yoo, A.V. McCormick, R.L. Penn, A. Stein, M. Tsapatsis, *Nat. Mater.* **7**, 984 (2008).
20. T. Yokoi, Y. Sakamoto, O. Terasaki, Y. Kubota, T. Okubo, T. Tatsumi, *J. Am. Chem. Soc.* **128**, 13664 (2006).
21. M.A. Snyder, J.A. Lee, T.M. Davis, L.E. Scriven, M. Tsapatsis, *Langmuir* **23**, 9924 (2007).
22. B. Fang, M.-S. Kim, J.H. Kim, S. Lim, J.-S. Yu, *J. Mater. Chem.* **20**, 10253 (2010).
23. M.H. Kim, S.H. Im, O.O. Park, *Adv. Funct. Mater.* **15**, 1329 (2005).
24. G. Singh, S. Pillai, A. Arpanaei, P. Kingshott, *Adv. Funct. Mater.* **21**, 2556 (2011).
25. E.C.M. Vermolen, A. Kuijk, L.C. Filion, M. Hermes, J.H.J. Thijssen, M. Dijkstra, A. van Blaaderen, *Proc. Natl. Acad. Sci. U.S.A.* **106**, 16063 (2009).
26. S.-C. Kung, C.-C. Chang, W. Fan, M.A. Snyder, *Langmuir* **30**, 11802 (2014).
27. Y. Kuroda, Y. Sakamoto, K. Kuroda, *J. Am. Chem. Soc.* **134**, 8684 (2012).
28. M. Fu, A.L. Zhao, D.W. He, Y.S. Wang, *Chem. Mater.* **26**, 3084 (2014).
29. S.G. Rudisill, N.M. Hein, D. Terzic, A. Stein, *Chem. Mater.* **25**, 745 (2013).
30. S.G. Rudisill, S. Shaker, D. Terzic, R. Le Maire, B.L. Su, A. Stein, *Inorg. Chem.* **54**, 993 (2015).
31. M. Fu, J. Zhou, B. Li, X. Huang, Y. Wang, L. Li, *J. Mater. Chem.* **18**, 5986 (2008).
32. M. Fu, J. Zhou, Q.F. Xiao, B. Li, R.L. Zong, W. Chen, J. Zhang, *Adv. Mater.* **18**, 1001 (2006).
33. P.D. Yang, T. Deng, D.Y. Zhao, P.Y. Feng, D. Pine, B.F. Chmelka, G.M. Whitesides, G.D. Stucky, *Science* **282**, 2244 (1998).
34. F. Li, Z. Wang, N.S. Ergang, C.A. Fyfe, A. Stein, *Langmuir* **23**, 3996 (2007).
35. L. Song, D. Feng, N.J. Fredin, K.G. Yager, R.L. Jones, Q. Wu, D. Zhao, B.D. Vogt, *ACS Nano* **4**, 189 (2010).
36. E. Huang, L. Rockford, T.P. Russell, C.J. Hawker, *Nature* **395**, 757 (1998).
37. X. Zheng, Y. Lv, Q. Kuang, Z. Zhu, X. Long, S. Yang, *Chem. Mater.* **26**, 5700 (2014).
38. Z. Zhang, F. Zuo, P. Feng, *J. Mater. Chem.* **20**, 2206 (2010).
39. E.J.W. Crossland, N. Noel, V. Sivaram, T. Leijtens, J.A. Alexander-Webber, H.J. Snaith, *Nature* **495**, 215 (2013).
40. B.T. Yonemoto, Q. Guo, G.S. Hutchings, W.C. Yoo, M.A. Snyder, F. Jiao, *Chem. Commun.* **50**, 8997 (2014).
41. S.B. Yoon, G.S. Chai, S.K. Kang, J.S. Yu, K.P. Gierszal, M. Jaroniec, *J. Am. Chem. Soc.* **127**, 4188 (2005).
42. Y. Jiao, D. Han, L. Liu, L. Ji, G. Guo, J. Hu, D. Yang, A. Dong, *Angew. Chem. Int. Ed.* **54**, 5727 (2015).
43. J.-H. Kim, J.-H. Kim, K.-H. Choi, H.K. Yu, J.H. Kim, J.S. Lee, S.-Y. Lee, *Nano Lett.* **14**, 4438 (2014).
44. Z. Tian, M.A. Snyder, *Langmuir* **30**, 12411 (2014).
45. B. Hatton, L. Mishchenko, S. Davis, K.H. Sandhage, J. Aizenberg, *Proc. Natl. Acad. Sci. U.S.A.* **107**, 10354 (2010).
46. L. Mishchenko, B. Hatton, M. Kolle, J. Aizenberg, *Small* **8**, 1904 (2012).
47. Y. Vasquez, M. Kolle, L. Mishchenko, B.D. Hatton, J. Aizenberg, *ACS Photonics* **1**, 53 (2013).
48. W.H. Guo, M. Wang, W. Xia, L.H. Dai, *Langmuir* **29**, 5944 (2013).
49. B. Mandlmeier, N.K. Minar, J.M. Feckl, D. Fattakhova-Rohlfing, T. Bein, *J. Mater. Chem. A* **2**, 6504 (2014).
50. R. Kubrin, J.J. do Rosario, H.S. Lee, S. Mohanty, R.P. Subrahmanyam, I. Smirnova, A. Petrov, A.Y. Petrov, M. Eich, G.A. Schneider, *ACS Appl. Mater. Interfaces* **5**, 13146 (2013).
51. Y. Jiao, D. Han, Y. Ding, X. Zhang, G. Guo, J. Hu, D. Yang, A. Dong, *Nat. Commun.* **6**, 6420 (2015).
52. H. Chen, J. Wydra, X. Zhang, P.-S. Lee, Z. Wang, W. Fan, M. Tsapatsis, *J. Am. Chem. Soc.* **133**, 12390 (2011).
53. P.-S. Lee, X. Zhang, J.A. Stoeger, A. Malek, W. Fan, S. Kumar, W.C. Yoo, S. Al Hashimi, R.L. Penn, A. Stein, M. Tsapatsis, *J. Am. Chem. Soc.* **133**, 493 (2011).
54. L. Li, X. Jiao, D. Chen, B.V. Lotsch, C. Li, *Chem. Mater.* **27**, 7601 (2015).
55. H.J. Cho, P. Dornath, W. Fan, *ACS Catal.* **4**, 2029 (2014).
56. M. Retsch, U. Jonas, *Adv. Funct. Mater.* **23**, 5381 (2013). □

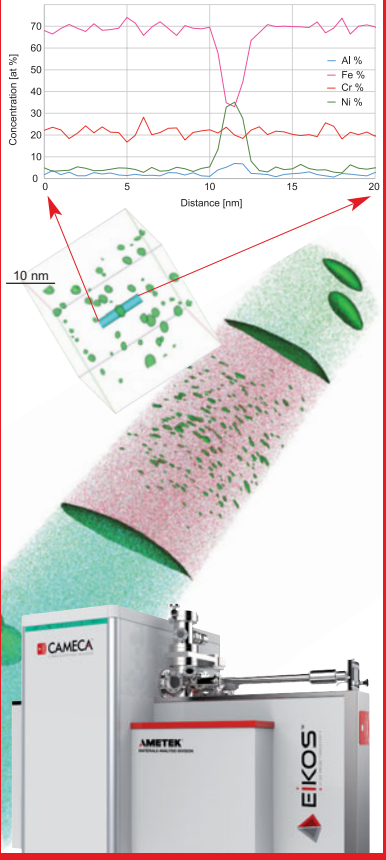
New from CAMECA!

EIKOS™
ATOM PROBE TOMOGRAPHY

The Accessible
Atom Probe

Building on 30 years of success in APT instrumentation & application, CAMECA announces EIKOS™, the Atom Probe microscope that enables routine 3D nano-analysis for both research & industry.

Analysis of an iron-based superalloy with EIKOS Atom Probe demonstrating microscale imaging capabilities with nanoscale chemical resolution.



Request your EIKOS information kit:
www.cameca.com/new/eikos.aspx
or cameca.info@ametek.com

CAMECA SCIENCE & METROLOGY SOLUTIONS
AMETEK MATERIALS ANALYSIS DIVISION

https://doi.org/10.1557/mrs.2016.187 Published online by Cambridge University Press